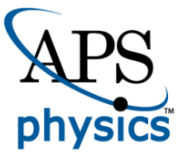

Elastogranular Mechanics: Buckling, Jamming, and Structure Formation

David J. Schunter, Jr., Martin Brandenbourger, Sophia Perriseau, and Douglas P. Holmes

Phys. Rev. Lett. **120**, 078002 — Published 14 February 2018

DOI: 10.1103/PhysRevLett.120.078002

Elastogranular Mechanics: Buckling, Jamming, and Structure Formation

David J. Schunter Jr., Martin Brandenbourger, Sophia Perriseau, and Douglas P. Holmes[1]

[1] *Mechanical Engineering, Boston University, Boston, MA, 02215, USA*

(Dated: January 8, 2018)

Confinement of a slender body into a granular array induces stress localization in the geometrically nonlinear structure, and jamming, reordering, and vertical dislodging of the surrounding granular medium. By varying the initial packing density of grains and the length of a confined *elastica*, we identify the critical length necessary to induce jamming, and demonstrate how folds couple with the granular medium to localize along grain boundaries. Above the jamming threshold, the characteristic length of *elastica* deformation is shown to diverge in a manner that is coupled with the motion and rearrangement of the grains, suggesting the ordering of the granular array governs the deformation of the slender structure. However, over confinement of the *elastica* will vertically dislodge grains, a form of stress relaxation in the granular medium that illustrates the intricate coupling in elastogranular interactions.

PACS numbers: 45.70.-n, 46.32.+x, 62.20.mq

Consider the growth of an elastic rod within a granular medium. As the rod elongates in a confined space, it will bend to minimize its internal energy [1, 2], reordering the surrounding granular material to accommodate higher arc length configurations. At low packing densities, the rod feels little resistance from the grains [3], while as the packing density is gradually increased to the point of jamming, the granular material begins to exert a large, inhomogeneous stress distribution on the elastic rod [4–8], deforming the geometrically nonlinear structure. It is well-known that slender structures will localize stress in response to a homogeneous stress distribution. Wrinkled sheets on a fluid substrate exhibit a spontaneous up–down symmetry breaking that tends toward an asymptotic isometry [9–13], while wrinkled sheets on an elastic substrate exhibit a period doubling instability and subsequent up–down symmetry breaking characterized by a subharmonic mode [14, 15]. The nonlinear response of slender structures to inhomogeneous stress distributions via coupling with discrete media is less well understood, despite occurring frequently in the natural world [16–18]. Stresses exerted by soil on a growing root can dictate growth pathways [19–21] and induce chiral, helical buckling [22–24]. Further, in dry sand environments, sand vipers can burrow [25], and desert–dwelling sandfish can swim within a granular bed by propagating an undulatory traveling wave down their rod–like bodies, enabling non-inertial swimming [26].

These coupled, *elastogranular* mechanics have generally been considered as local inhomogeneities or studied in systems where the length scale of elastic deformation exceeds by several orders of magnitude the grain size. The question of how granular ordering can influence deformation of a slender body, such as an elastica, has remained open. In this Letter, we describe the connections between jamming, ordering, and stress localization in an elastogranular system through the use of simple scaling arguments, and the observation of the relaxation

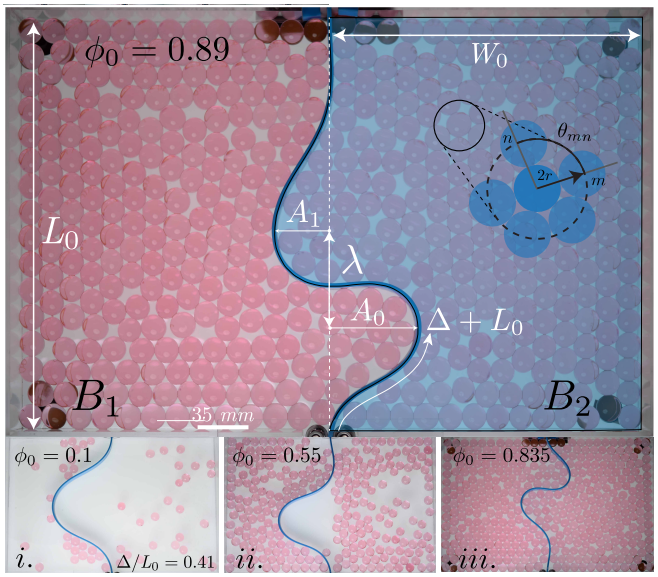

FIG. 1. Shape profiles of the elastica as additional arc length Δ is injected into a granular array of length L_0, width W_0 over a range of initial experimental packing fractions: $\phi_0 = 0.1$ (i), $\phi_0 = 0.55$ (ii), $\phi_0 \approx \phi_j = 0.835$ (iii).

of stresses within the granular network through the vertical dislodging of grains. These results will help to illuminate the ways slender elastic structures interact with non-homogeneous and fragile media, behavior commonly seen in plant root growth [24], the piercing of soft tissue [27], and the reinforcement of jammed granular architectures [28, 29].

To understand how the discrete, heterogenous behavior of a granular medium couples with the nonlinear deformation of a slender continuum structure, we experimentally considered the confinement of a planar elastica within a 2D monolayer of soft, nearly frictionless spherical grains. Individual packings are prepared by randomly populating both sides of an initially straight, undeformed elastic beam, with N approximately monodisperse grains (*see Supplemental Material in [30]), such that the initial

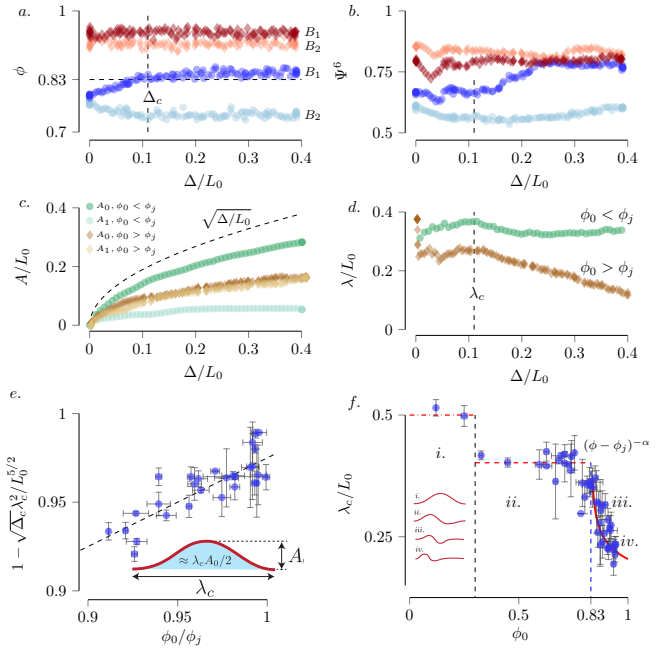

FIG. 2. Changes in (a) packing fraction ϕ, (b) bond-orientation order Ψ^6, (c) primary and second amplitude A_0 and A_1, and (d) peak-to-peak distance between amplitudes λ, in both pre (blue points) and post-jammed (red diamonds) systems as the elastica is injected (Δ/L_0). Two characteristic lengths are seen to emerge: (e) a critical injected arc length of elastica Δ_c necessary to induce jamming in a 2D granular array, and (f) the length of the confinement region λ_c in which the elastica will localize curvature, as a function of packing fraction.

packing fraction, $\phi_i = \pi N r^2/B_i$, where $r = 8.9 \pm 0.4$ mm is the average grain radius, N is the number of grains, and B_i is the area of the i^{th} side ($i = 1, 2$), is the same on either side. Prior to each run, the particles were mechanically agitated, then allowed to settle to remove any hysteretic effects. The geometrically nonlinear behavior of the elastica is dependent on bending rigidity per unit width, $Eh^3/12$, where E is Young's elastic modulus, and h is thickness. Elastic instabilities and subsequent stress localization in flexible rods are generally characterized by a region of maximum curvature, $\kappa_m \sim A_0/\lambda^2$, where A_0 is the primary amplitude, and λ is an effective buckling length. Here, we define λ as the distance between the two primary maxima of deformation A_0 and A_1 (see Fig. 1) [31]. We first quantify the elastogranular interactions as the elastica's arc length was increased by a length Δ in a quasi–static manner from an initial length L_0 for a range of initial packing fractions ϕ_0 (Fig. 1*i.*–*iii.*).

An elastica, clamped at its ends within fixed boundaries, adopts a cosine–like deflection profile when injected into a low density granular array, *i.e.* $\phi_0 \lesssim 0.3$ (see Fig. 1i.), with its exact shape being governed by an elliptic integral [32]. At larger packing fractions, $0.3 \lesssim \phi_0 < \phi_j$, the post-buckling geometry of the elastica breaks the initial left–right symmetry between areas B_1 and B_2 with a maximum amplitude that grows as $A_0/L_0 \sim \sqrt{\Delta/L_0}$ (Fig. 2c). The packing fraction on the side containing A_0 increases, this subsystem eventually reaching a jammed state at a critical packing fraction $\phi_j = 0.8305 \pm 0.0135$ [30], and a critical elongation Δ_c (Fig. 2a – blue circles). Reordering of the granular array, characterized by the global bond orientation parameter $\Psi^6 = \left| N^{-1} \sum_{m=1}^{N} N_b^{-1} \sum_{n=1}^{N_b} e^{6i\theta_{mn}} \right|$, occurs following the onset of jamming (Fig. 2b – blue circles), along with a slight drop in normalized distance between maxima, λ/L_0 (Fig. 2d – green circles). Following this reordering, λ values are seen to remain constant as additional arc length is injected into the system. Once a jammed state is reached (see Fig. 1iii.), the packing fraction remains constant as the elastica's arc length is increased. In high density granular assemblies, (*i.e.* $\phi_0 \geq \phi_j$), the elastica buckles in an antisymmetric mode two shape, with peaks (A_0 and A_1) of similar amplitude (Fig. 2b – red diamonds). To accommodate increasing Δ, localized disturbances and disaggregation of the granular array occurs in the neighborhood of both A_0 and A_1 (Fig. 2b – red diamonds). In what follows, we establish a physical model to describe these characteristic elastogranular behaviors.

We begin by describing Δ_c, the arc length of elastica necessary to induce jamming in a packing with $\phi_0 < \phi_j$. For the range of experimentally prepared packings, we find that the initial half wavelength λ remains essentially constant at low injection, when $\Delta/L_0 < 0.1$. This consistency at low Δ across all investigated packing fractions suggests that we may be able to probe our system for a linearly derived length scale, an approach utilized in both simulations and experiments of 2D granular systems [33–37]. From this linear regime, we define a characteristic length λ_c as the average of λ for $0 < \Delta/L_0 < 0.1$. For low Δ and initial packing fractions $\phi_0 < \phi_j$, the elastica exhibits a primarily mode one shape. Recalling that the primary amplitude scales as $A_0/\lambda \sim \sqrt{\Delta/L}$, we approximate the buckled elastica as a triangle of base λ_c and height A_0 (inset Fig. 2e). As the area on one side of the array is reduced by $\frac{1}{2}\lambda_c^2\sqrt{\Delta/L}$, the packing fraction as a function of Δ may be written as $\phi(\Delta) = \pi r^2 N/(L_0 W_0 - \frac{1}{2}\lambda_c^2\sqrt{\Delta/L})$. It follows that by separating the initial packing fraction ϕ_0, and considering the array at jamming, where $\phi \to \phi_j$ and $\Delta \to \Delta_c$, we arrive at a critical length of elastica needed to jam a 2D array of soft, nearly frictionless spherical grains, *i.e.* an effective *elastogranular* length,

$$\frac{\Delta_c}{L_0} \sim \left(\frac{L_0}{\lambda_c}\right)^4 \left[1 - \frac{\phi_0}{\phi_j}\right]^2. \qquad (1)$$

Equation 1 is plotted with a slope of 1/2 in Fig. 2e along with individual packings that jammed at a critical arc length Δ_c, and captures the critical length to induce jamming very well. This characteristic length is analogous to a length scale recently found to describe the onset of

bending of an elastic filament within a granular flow [8].

Beyond the jamming threshold, the elastica always localizes deformation over a finite length smaller than L_0 (Fig. 2f), similar to its behavior on a homogenous elastic foundation [9–12, 38]. Notably, this length diverges when it approaches the jamming packing fraction. Empirically, we can characterize our system by

$$\lambda_c \sim \frac{1}{(\phi - \phi_j)^{\alpha}}. \tag{2}$$

Eq. 2 best fits our measurements for $\alpha = 0.185$ [30]. Previous publications have already reported the observation of diverging length scales in disordered granular media subject to local stimuli, both experimentally [39] and via simulations [33, 35, 40, 41]. In our experiments, high packing fractions and monodisperse grains give rise to a highly ordered granular array globally, while grains near the localized deformation of the elastica tend to be disordered [30]. These disordered grains are the most likely to recirculate to accommodate additional elastica arc length [42]. As the packing fraction increases, the maximum number of disordered grains that can recirculate must necessarily decrease, presenting an area of characteristic size λ_g available for the elastic to deform within. Therefore, we look for a similar relationship between λ_g and $\phi - \phi_j$ in the granular arrays by measuring the granular displacement field that arises via the initial buckling of the elastic rod. By measuring the characteristic length of grain motion λ_g, we find a similar diverging length scale near jamming, such that $\lambda_g \sim (\phi - \phi_j)^{-\beta}$, with $\beta = 0.19$ [30] [43]. The similarity in these exponents suggests that as the elastic rod locally applies a force on the granular media, it is limited in its own deformation range due to the propagation of these forces through the grains.

To understand how the local packing and order of the granular array influences the shape of the confined elastica, we compare the elastica shape and granular ordering of two typical experiments ($\phi_0 = 0.70$ and $\phi_0 = 0.90$) in Fig. 3a, where each grain is colored by a measure of its local bond orientation number, $\psi_m^6 = N_b^{-1} \sum_{n=1}^{N_b} e^{6i\theta_{mn}}$. In the non-jammed array, the grains move freely to accommodate the growing amplitudes of the elastica, while jammed arrays must rearrange to accommodate the growing elastica. In Fig. 3a (when $\phi_0 = 0.90$), regions near the fixed end of the elastica are surrounded by hexagonally packed grains [44]. Bound by these regions, whose geometry is seen to match that of a 2D hexagonal unit cell, elastica deformations tend towards an antisymmetric, overlapping fold – a shape expected for large folds on fluid interfaces, but not commonly observed [45]. Notably, λ remains constant for $\phi < \phi_j$, yet decreases for $\phi \geq \phi_j$.

We confirm this by plotting A_0/λ as a function of $\sqrt{\Delta/L}$ over a range of initial packing fractions in Fig. 3c. For all ϕ_0 and $\Delta/L < 0.3$, the normalized amplitude

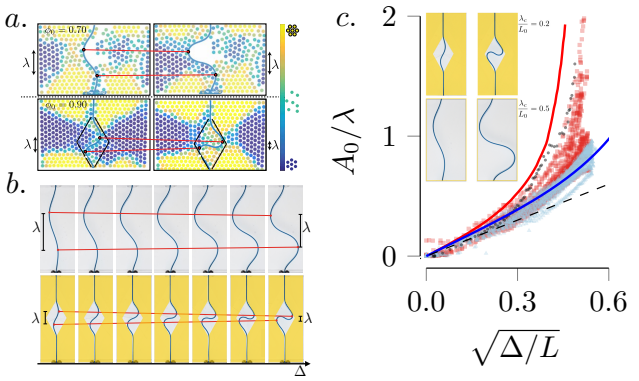

FIG. 3. (a) For $\phi_0 < \phi_j$, the elastica buckles to one side of the enclosure, inducing jamming at a critical injection length Δ_c. At $\phi_0 \geq \phi_j$, antisymmetric folding of the elastica occurs within a lozenge shaped region of the granular array. (b) Model experiments demonstrate how crystalline structures in the granular media effectively act as a rigid boundary, confining the elastica. (c) A_0/λ as a function of $\sqrt{\Delta/L}$. For $\phi < \phi_j$ (blue triangles), deformations follow the shape of a free elastica (blue solid line), while above jamming ($\phi > \phi_j$, red squares), the presence of an upper bound (corresponding to lozenge crystal structure), confines the elastica. This upper limit was verified both experimentally (black circles) and numerically (red line).

scales linearly with $\sqrt{\Delta/L}$ (Fig. 3c – dashed black line), which is consistent with the definition of λ_c. At larger confined lengths, the ratio of amplitude to wavelength strongly depends on whether the elastica is injected into a loose (blue triangles) or jammed (red squares) granular state. Within a loose granular array A_0/λ follows the shape of the antisymmetric, nonlinear elastica (Fig. 3c – solid blue line) [30, 32]. The ratio of A_0/λ rapidly diverges from the classical behavior when the elastica elongates within a jammed array.

As a granular medium transitions from below jamming to a marginally stable jammed state, collective decreases in interparticle distance lead to the development of heterogeneous force chains between contacting particles [46, 47]. In the case of a monodisperse medium, this results in local crystal structures that are difficult to deform, and these crystals act to effectively constrain the elastica's deformation. To illustrate this effect, we show experimental results for two extreme cases: an elastica buckled in mode two that can either (i.) freely elongate within the granular medium, or (ii.) be completely confined in a crystalline geometry imposed by the grains (Fig. 3b). In the second case, we used rigid walls that correspond to four local hexagonal crystals surrounding the elastic beam, forming a 60 degree angle with the horizontal, and creating a lozenge–like shape of characteristic length λ_g. This limiting case is similar to the shape of the compacted region described by Kolb *et al.* [42], and is partially illustrated by Fig. 3a. (see black lines), where we observe the elastica surrounded by granular crystals, which appear yellow in Fig. 3a. As the initial buckling

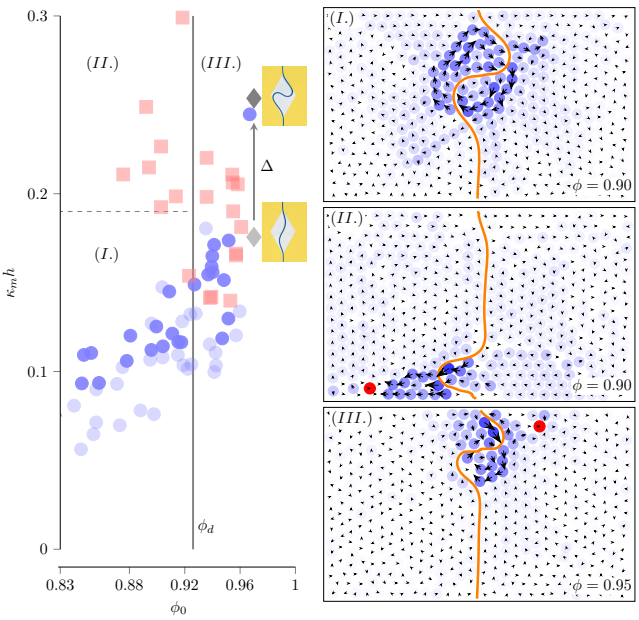

FIG. 4. (a) Maximum curvature of the elastica normalized by its thickness $\kappa_m h$, as a function of the initial packing fraction ϕ_0. The light and dark blue circles describe $\kappa_m h$ for an injected arc length $\Delta/L_0 = 0.1$ and 0.41, respectively. Red squares correspond to $\kappa_m h$ preceding a dislodging event. The light and dark gray diamonds correspond to measurements from experiments with rigid boundaries (see associated images). System behavior described by three distinct regions (I, II, III). (b) Examples of the vector fields of granular displacements for each region. Grain opacity corresponds to the norm of their vector displacement.

of the elastic beam depends on the packing fraction, we chose the minimum observed value of λ_c as the characteristic length of our confinement. We confirm that confinement within this space represents an upper bound on the diverging ratio of A_0/λ via experiments (image sequence Fig. 3b and black points Fig. 3c) and by numerically solving the equation for an elastica buckling within a lozenge–shaped void (red line Fig. 3c) [30]. These results suggest a means for studying the localization of elastic structures within more complex granular configurations, as different geometrically limiting cases will emerge.

It appears from Fig. 3c that the elastica governs the elastogranular behavior when $\phi < \phi_j$, while the granular array governs the behavior when $\phi \geq \phi_j$, however this trend breaks down at high packing fractions or in rare cases where we observe highly localized elastica folds. At large enough confinement, the granular monolayer can yield by vertically dislodging a grain [48]. In Fig. 4, we plot the maximum curvature of the elastica normalized by its thickness, $\kappa_m h$, as a function of the grains packing fraction ϕ for a short and a long injected arc length ($\Delta/L_0 = 0.11$ and 0.41 for the light and dark blue circles, respectively), and indicate the curvature at which a grain was dislodged (red squares). We note three regions in this plot. In region I, we observe an equilibrium elastica shape, and no grain dislodgings. Tracking the displacement vectors of each grain for a characteristic experiment in this region, we see that a high number of grains close to the primary maxima A_0 and A_1 tend to displace (Fig. 4I). Granular configurations can force the elastica to localize with a high curvature, and because we observe granular motion tending to focus in a given direction, the highly curved beam can act like a point force within the array (Fig. 4II). At the same packing fraction, we sometimes observe more highly confined elastica shapes composed of folds of high curvature, which can induce dislodging within the granular array (Fig. 4II). Finally, beyond a critical packing fraction, dislodging events appear to be independent of $\kappa_m h$ (Fig. 4III). To understand the role of packing fraction on dislodging, we homogeneously reduced the area occupied by a monolayer of grains absent of an elastica, and measured ϕ at the first dislodging event. A small perturbation beyond a critical packing fraction of $\phi_d = 0.926$ (black vertical line) dislodges a grain, suggesting that the appearance of dislodgings indicate the packing limit of these soft beads [49]. Here again we observe a similar granular displacement field as seen in region I, though confined to a smaller region as expected from equation 2.

The wealth of elastogranular behaviors observed here indicate an intricate coupling between geometrically nonlinear slender bodies and heterogenous, fragile matter. The confinement and deformation of the slender structure is highly dependent on the proximity of the granular array to the jamming point, yet the competition between the structure's elastic energy and the granular matter's local order gives rise to a variety of elastogranular behaviors (notably antisymmetric/overlapping folds and a deformation length scale proportional to packing fraction) that can be observed across a range of packing fractions and confined lengths. These results will bring new insight into the behavior of deformable structures within granular matter, colloidal systems, and soft gels, and will be relevant to modeling root growth and developing smart, steerable needles.

DPH and DJSJ acknowledge the financial support from NSF CMMI – CAREER through Mechanics of Materials and Structures (#1454153). MB acknowledges the financial support from BAEF. DPH thanks Frederic Lechenault and Evelyne Kolb for helpful discussions and inspiration. We also thank Osiagwe Osman for performing preliminary experiments, Michele Curatolo for his guidance on numerical implementation and Abdikhalaq Bade for his assistance implementing the particle image velocimetry to track the granular motion.

[1] B. Audoly and Y. Pomeau, *Elasticity and geometry: from hair curls to the non-linear response of shells* (Oxford

University Press, 2010).
[2] R. Capovilla, C. Chryssomalakos, and J. Guven, Journal of Physics A: Mathematical and General **35**, 6571 (2002).
[3] A. J. Liu and S. R. Nagel, Nature **396**, 21 (1998).
[4] P. Dantu, Géotechnique **18**, 50 (1968).
[5] C. Liu, S. R. Nagel, D. Schecter, S. Coppersmith, S. Majumdar, *et al.*, Science **269**, 513 (1995).
[6] S. Coppersmith, C.-h. Liu, S. Majumdar, O. Narayan, and T. Witten, Phys. Rev. E **53**, 4673 (1996).
[7] C. S. O'Hern, S. A. Langer, A. J. Liu, and S. R. Nagel, Phys. Rev. Lett. **86**, 111 (2001).
[8] N. Algarra, P. Karagiannopoulos, A. Lazarus, D. Vandembroucq, and E. Kolb, arXiv preprint arXiv:1708.02162 (2017).
[9] L. Pocivavsek, R. Dellsy, A. Kern, S. Johnson, B. Lin, K. Y. C. Lee, and E. Cerda, Science **320**, 912 (2008).
[10] D. P. Holmes and A. J. Crosby, Phys. Rev. Lett. **105**, 038303 (2010).
[11] H. Diamant and T. A. Witten, Phys. Rev. Lett. **107**, 164302 (2011).
[12] M. Rivetti and S. Neukirch, J Mech Phys Solids **69**, 143 (2014).
[13] D. Vella, J. Huang, N. Menon, T. P. Russell, and B. Davidovitch, Phys. Rev. Lett. **114**, 014301 (2015).
[14] F. Brau, H. Vandeparre, A. Sabbah, C. Poulard, A. Boudaoud, and P. Damman, Nature Phys. **7**, 56 (2011).
[15] F. Brau, P. Damman, H. Diamant, and T. A. Witten, Soft Matter **9**, 8177 (2013).
[16] T. A. Sobral and M. A. F. Gomes, J. Phys. D: Appl. Phys **48**, 335305 (2015).
[17] A. R. Mojdehi, B. Tavakol, W. Royston, D. A. Dillard, and D. P. Holmes, Extreme Mech. Lett. (2016).
[18] B. J. Gurmessa and A. B. Croll, Soft matter **13**, 1764 (2017).
[19] A. G. Bengough, M. F. Bransby, J. Hans, S. J. McKenna, T. J. Roberts, and T. A. Valentine, J. Exp. Bot. **57**, 437 (2006).
[20] E. Kolb, C. Hartmann, and P. Genet, Plant Soil **360**, 19 (2012).
[21] E. Kolb, V. Legue, and M.-B. Bogeat-Triboulot, Physical Biology (2017).
[22] G. Whiteley, J. Hewitt, and A. Dexter, Physiol. Plant. **54**, 333 (1982).
[23] M. Oliva and C. Dunand, New Phytol **176**, 37 (2007).
[24] J. L. Silverberg, R. D. Noar, M. S. Packer, M. J. Harrison, C. L. Henley, I. Cohen, and S. J. Gerbode, PNAS **109**, 16794 (2012).
[25] B. A. Young, M. Morain, and R. Wood, Copeia **2003**, 131 (2003).
[26] R. D. Maladen, Y. Ding, C. Li, and D. I. Goldman, science **325**, 314 (2009).
[27] V. Choumet, T. Attout, L. Chartier, H. Khun, J. Sautereau, A. Robbe-Vincent, M. H. P. Brey, and O. Bain, PLoS ONE **7**, e50464 (2012).
[28] H. J. H. M. Fauconneau, F. K. Wittel, Granular Matter **18**, 1 (2016).
[29] P. Aejmelaeus-Lindström, J. Willmann, S. Tibbits, F. Gramazio, and M. Kohler, Granular Matter **18**, 1 (2016).
[30] The Supplemental Information (SI) can be found online at: (2017).
[31] This is motivated by the high regularity of anti-symmetric mode two shapes that were observed at full injected arc length. The Cartesian peak–to–peak distance provided more detail about the system than the curvilinear distance [30].
[32] D. Bigoni *et al.*, *Extremely Deformable Structures*, Vol. 562 (Springer, 2015).
[33] W. G. Ellenbroek, M. van Hecke, and W. van Saarloos, Physical Review E **80**, 061307 (2009).
[34] C. P. Goodrich, W. G. Ellenbroek, and A. J. Liu, Soft Matter **9**, 10993 (2013).
[35] M. Wyart, L. E. Silbert, S. R. Nagel, and T. A. Witten, Phys. Rev. E **72**, 051306 (2005).
[36] S. S. Schoenholz, C. P. Goodrich, O. Kogan, A. J. Liu, and S. R. Nagel, Soft Matter **9**, 11000 (2013).
[37] W. G. Ellenbroek, E. Somfai, M. van Hecke, and W. van Saarloos, Physical review letters **97**, 258001 (2006).
[38] M. Hetényi, *Beams on Elastic Foundation: Theory with Applications in the Fields of Civil and Mechanical Engineering* (University of Michigan press, 1946).
[39] C. Coulais, A. Seguin, and O. Dauchot, Physical review letters **113**, 198001 (2014).
[40] G. D. E. Lerner, E. Degiuli and M. Wyat, Soft Matter **10**, 5085 (2014).
[41] M. Van Hecke, J. Phys. Condens. Matter **22**, 033101 (2009).
[42] E. Kolb, P. Cixous, N. Gaudouen, and T. Darnige, Physical Review E **87**, 032207 (2013).
[43] As shown in [30], λ_g corresponds to the length over which grains around the elastica are disordered.
[44] S. Torquato and F. Stillinger, J. Phys. Chem. B **105**, 11849 (2001).
[45] V. Démery, B. Davidovitch, and C. D. Santangelo, Phys. Rev. E **90**, 042401 (2014).
[46] T. S. Majmudar and R. P. Behringer, Nature **435**, 1079 (2005).
[47] A. R. van Eerd, W. G. Ellenbroek, M. van Hecke, J. H. Snoeijer, and T. J. Vlugt, Physical Review E **75**, 060302 (2007).
[48] A. Tordesillas, D. Carey, A. B. Croll, J. Shi, and B. Gurmessa, Granular Matter **16**, 249 (2014).
[49] The experimentally determined ϕ_d is larger than the hexagonal packing limit of $\phi_h = 0.907$, and is likely due to the deformability and slight polydispersity of the grains.
[50] H. Singh and J. Hanna, arXiv preprint arXiv:1706.03047 (2017).